ELSEVIER

Chemical Engineering Science 59 (2004) 2547–2565

Chemical Engineering Science

www.elsevier.com/locate/ces

Solution of the droplet breakage equation for interacting liquid–liquid dispersions: a conservative discretization approach

Menwer M. Attarakih[a], Hans-Jörg Bart[a,*], Naim M. Faqir[b]

[a] *Faculty of Mechanical and Process Engineering, Institute of Process Engineering, The University of Kaiserslautern, P.O. Box: 3049, Kaiserslautern D-67653, Germany*

[b] *The University of Jordan, Faculty of Engineering and Technology, Chemical Engineering Department, Amman 11942, Jordan*

Received 2 June 2003; received in revised form 2 March 2004; accepted 5 March 2004

Abstract

A conservative discretization approach for the population balance equation (PBE) with only droplet breakage describing the hydrodynamics of a continuously interacting liquid–liquid dispersion is presented. The approach is conservative in the sense that it conserves any two integral properties associated with the number droplet distribution and thus it is considered internally consistent. The discrete set of equations is laid down through applying the subdomain method where it is shown that this set of discrete equations is only internally consistent with respect to one integral property. The internal consistency is enforced by introducing a set of two auxiliary functions that are uniquely determined by matching the integral properties obtainable from the discrete set against those from the continuous PBE. However, it is shown that this conservation of integral properties is not exact for all the subdomains and hence it results in what we call the intrinsic discretization error (IDE). This IDE is not only associated with this approach, but also it is found inherently existing in the fixed-pivot (FP) technique of Kumar and Ramkrishna (Chem. Eng. Sci. 51 (1996a) 1333). The derived equations of the IDE for the present discretization approach and the FP technique generalized to continuous flow systems show that the present approach enjoys a small value of the IDE. To validate the discretization approach, two analytical solutions for the continuous PBE are presented, where good agreement is found between the predicted and the analytical solutions. To assess the reliability of the present discretization approach two experimentally validated breakage frequency functions describing droplet breakage in a turbulent continuous phase as well as two daughter droplet distributions are considered. The convergence characteristics show that the present discretization approach has an identical convergence rate as that of the FP technique, and in some cases it is superior to it. This rate of convergence is found approximately proportional to the square of the inverse of the number of subdomains.

Keywords: Liquid–liquid dispersion; Hydrodynamics; Droplet breakage; Population balance; Intrinsic discretization error; Numerical Simulation

1. Introduction

The population balance approach is now being successfully used to model the complex behavior of the dispersed phase in many of chemical processes taking place in liquid systems. In these systems the population of droplets are considered to lose their identity due to many stochastic events and hence the internal properties (coordinates) of these droplets (such as size, concentration, age, ... etc.) are subject to inevitable changes during a given residence time period. These changes are due to the entry and exit events (for continuous flow systems), droplet breakage resulting from the interaction of a single liquid droplet and the turbulent continuous phase as well as the interaction of the continuous phase and any two droplets through coalescence. After a sufficiently long period of time, equilibria is reached between these events that result in a steady state distributions with respect to certain internal droplet coordinates such as size or concentration. Among these distributions is the droplet size distribution, which is very important in determining the total interfacial area that should be made available to mass and heat fluxes calculations. A conservation law that is able to describe such a complex behavior and hence the evolution of the droplet size distribution of the

* Corresponding author. Tel.: +49-631-205-2414; fax: +49-631-205-2119.

E-mail address: bart@mv.uni-kl.de (H. Bart).

0009-2509/$ - see front matter © 2004 Elsevier Ltd. All rights reserved.
doi:10.1016/j.ces.2004.03.004

dispersed phase is the population balance equation (PBE). This PBE could be written for a continuous flow system as follows (Ramkrishna, 2000):

$$\frac{\partial n(z,t)}{\partial t} + \nabla \cdot \left(\frac{\mathrm{d}z_i}{\mathrm{d}t} \cdot n(z,t) \right) = \frac{1}{\tau}\left(n^{\mathrm{feed}}(z,t) - n(z,t)\right) + \rho[\{n(z,t)\}; z, t], \quad (1)$$

where $n(z,t)$ is the average number of droplets per unit volume of the droplet phase space at location $\boldsymbol{z}$ and the time instant t. The independent variable, $\boldsymbol{z}$, is a vector of the droplet internal coordinates (z_i) such as droplet size, concentration, ... etc. and its external coordinates (spatial location). In the differential phase space $\boldsymbol{z}$ to $\boldsymbol{z} + \mathbf{d}\boldsymbol{z}$, the first term on the left-hand side of Eq. (1) represents the accumulation rate of the number of droplets, while the second term is the convective rate along the droplet internal coordinates. The first term on the right-hand side represents the net rate of the number of droplets per unit volume crossing the boundary of the continuous flow system in a specified residence time, τ. While the second term on the right-hand side represents the net rate of number of droplet generation $\rho\mathbf{d}\boldsymbol{z}$ per unit volume due to droplet breakage and coalescence.

Despite the importance of Eq. (1), it rarely has an analytical solution due to the relatively complex form of the source term, ρ, which has integral terms as we will show below. However, a few analytical solutions exist for a simple set of breakage and feed distribution functions where the convection term is neglected (McGrady and Ziff, 1988; Nicmanis and Hounslow, 1998). In general for realistic modeling of the breakage and coalescence phenomena it is not possible to find a general analytical solution, and hence a numerical approximation is sought.

Accordingly, the underlying idea of this work is to present a general, detailed, and conservative (by conserving any two integral properties associated with the number distribution) discretization approach to solve numerically the PBE for droplet breakage describing the hydrodynamics in a perfectly mixed continuous flow vessel. However, the generality of the approach does not restrict it to this type of process and it could be easily coupled with a suitable discretization approach such as the fixed-pivot technique of Kumar and Ramkrishna (1996a) for droplet coalescence. A special attention will be paid to the dynamic evolution of the droplet size distribution and it will be validated analytically by presenting two analytical dynamic solutions of the problem in hand through converting the integro-partial differential equation (IPDE) into an ODE with respect to the droplet size. Moreover, various combinations of the experimentally validated breakage functions from the published literature are used to asses the present approach.

2. The PBE for droplet breakage

In the present work we confine ourselves only to the hydrodynamic behavior of completely mixed continuous flow systems and the droplet convective rate is neglected (in the absence of mass transfer). Moreover, among the aforementioned stochastic events the droplet coalescence could be neglected at low concentration of the dispersed phase (lean dispersions) and hence droplet breakage is said to be dominant (Shah and Ramkrishna, 1973). These assumptions simplify Eq. (1) to

$$\frac{\partial n(v,t)}{\partial t} = \frac{1}{\tau}(n^{\mathrm{feed}}(v,t) - n(v,t)) - \Gamma(v)n(v,t) + \int_v^{v_{\max}} \Gamma(v')\beta_n(v|v')n(v',t)\,\mathrm{d}v', \quad (2)$$

where v is the droplet volume, Γ is the breakage frequency and β_n is the number distribution of the daughter droplets resulting from the breakage of a mother droplet of volume v'.

Normally, the droplet internal coordinate is chosen as the droplet diameter instead of volume as appears in Eq. (2). However, it is simpler to discretize the PBE in terms of droplet volume rather than diameter and then the discrete ODEs will be projected onto the droplet diameter coordinate.

The initial condition for the PBE equation, Eq. (2), is given by some initial distribution of the dispersed phase droplets $n(v,0) = n_0(v)$, while the boundary or the regulatory conditions for Eq. (2) could be obtained by considering the minimum and maximum droplet sizes prevailing in the interacting liquid–liquid dispersion at a given turbulent energy dissipation and a physicochemical properties. The maximum droplet size is needed such that negligible distribution of the droplets above this size exists. This could be estimated in terms of droplet diameter from the following correlation (Tsouris and Tavlarides, 1994):

$$d_{\max} = c_m \left(\frac{D_R}{We^{0.6}}\right)\left(1 + 2.5\phi\,\frac{\mu_d + 0.4\mu_c}{\mu_d + \mu_c}\right)^{1.2}, \quad (3)$$

where c_m is a constant whose accepted value is 0.125, We is the Weber number, ϕ is the dispersed phase hold up in the vessel, and μ_c and μ_d are the viscosities of the continuous and the dispersed phases, respectively. Actually, this correlation predicts the maximum droplet diameter that is prevailing in the turbulent dispersion inside the vessel. So, if a droplet of larger diameter than that predicted using Eq. (3) is fed into the vessel, then the following boundary condition takes it into account:

$$n(v > \max(v_{\max}, v_{\max}^{\mathrm{feed}}), t) = 0. \quad (4)$$

The minimum droplet size could be estimated if the assumption of a local dynamic equilibrium between breakage and coalescence is established. Accordingly, the droplets having diameter larger than $d_{\max}$ will break up and that smaller than $d_{\min}$ will coalesce. Based on this, Liu and Li (1999) derived an expression for the estimation of the minimum

droplet diameter:

$$d_{\min} = \left(\frac{\gamma^{1.38} B^{0.46}}{0.0272 \mu_c \rho_c^{0.84} \varepsilon^{0.89}} \right)^{1/3.11}, \quad (5)$$

where B is the London–van der Waals constant and ε is the energy dissipation. Since the coalescence is assumed to be negligible in this work, it is expected that $d_{\min}$ will be smaller than that predicted using Eq. (5). Moreover, if the minimum droplet diameter of the droplets fed to the vessel is less than that estimated from Eq. (5), then we could apply the following boundary condition at the small size range:

$$n(v < \min(v_{\min}, v_{\min}^{\text{feed}}), t) = 0. \quad (6)$$

Anyhow, the above relations will be very useful for initial estimations but the actual values of $d_{\min}$ and $d_{\max}$ will be estimated in the next sections based on the minimization of the total finite domain error (FDE) (Attarakih et al. 2003a).

3. Previous work

Many discretization techniques are proposed in the literature to approximate the PBE given by Eq. (2). These approximate methods could be categorized into two broad classes: zero and high order methods. In the first category the droplet internal coordinate (size) is divided into many intervals (classes) and the population in each interval is considered to behave like a concentrated single droplet (Nambiar et al., 1992, Hill and Ng, 1995, Kronberger, 1995; Kumar and Ramkrishna, 1996a,b; Ramkrishna, 2000; Vanni, 1999,2000). The second category approximates the size distribution function within each interval by a higher order polynomial (usually cubic) at certain nodal points at which the exact solution is approximated based either on the orthogonal collocation or the Galarkin methods. Although these methods are more accurate, they are expensive from the computational point of view and sometimes suffer from stability problems particularly when convection along the droplet internal coordinate is considered (Nicmanis and Hounslow, 1998; Mahoney and Ramkrishna, 2002). Several comprehensive reviews concerning the numerical techniques for the approximation of the PBE are available (Ramkrishna, 1985; Kostoglou and Karabelas, 1994; Kumar and Ramkrishna, 1996a; Vanni, 2000, Attarakih et al. (2004)).

The zero order methods could be further classified into three groups: the first two groups are classified according to the work of Kumar and Ramkrishna (1996a) depending on the way of closing the resulting set of equations due to discretization. The first class of this group is due to Gelbard et al. (1980) where they applied the mean value theorem of integrals on the number density function. The resulting discrete equations are a set of ODEs with many double integrals appearing inside the summations. These double integrals are considered to be computationally expensive especially when real time dependent breakage functions are encountered. Vanni (2000) extended the original work of these authors to droplet breakage. Beside the inefficiency due to the evaluation of the double integrals in each interval, the approach suffers from its conservation only of one integral property associated with the number distribution and hence making it less accurate as pointed out by Kumar and Ramkrishna (1996a), and Vanni (2000). Kronberger et al. (1995) used the Galerkin method with a set of zero order polynomials as the test and trial functions. Although the method is computationally attractive for a few time independent breakage and coalescence functions, it places a heavy computational load for such real time dependent functions. Moreover, the method is only consistent with respect to the conservation of the total droplet volume and the evaluation of the double integrals may encounter singularity problems as pointed out by Kronberger (1995) and Mahoney and Ramkrishna (2002). Through applying the mean value theorem of integrals on the breakage/coalescence frequency the second class of methods is laid down by Kumar and Ramkrishna (1996a) to obtain a closed set of ODEs. The resulting method is free of evaluation of the double integrals in each interval. This approach is called the fixed-pivot technique and has the advantage of being flexible to conserve any two integral properties associated with the number distribution. Vanni (2000) showed that this technique offers a robust and versatile solver for the PBE by applying it successfully to 11 case studies. Attarakih et al. (2003b, 2004) generalized the fixed-pivot technique to solve numerically the PBE describing the hydrodynamics in differential liquid–liquid contactors. The present authors exploited the special structure of this technique to decouple the time dependent variables from the breakage and coalescence frequency functions by introducing the idea of breakage and coalescence matrices. This makes it possible to generate these matrices off-line and only once a time thus reducing dramatically the computational time particularly when the sparse structure of the coalescence matrix is taken into consideration.

Within the same framework, Kumar and Ramkrishna (1996b) developed a more accurate approach than the fixed-pivot technique, which they called the moving-pivot technique. The technique has the advantage of conserving any two specific integral properties by simultaneously solving for example the number and the volume (mass) balances. These equations are coupled through the representative droplets volumes, which allowed moving to satisfy both balances. The technique was tested only for droplet coalescence in a batch vessel and the numerical results showed a superior performance when compared to the fixed-pivot technique. However, it is only recently that the moving-pivot technique for droplet breakage is tested and extended to continuous flow systems by Attarakih et al. (2002, 2003a,b, 2004). In spite of its remarkable accuracy the technique has a drawback of being computationally expensive due to the continuous change of the droplet representative sizes and hence call for repeated evaluations of the breakage and coalescence functions.

Ribeiro et al. (1995) introduced a simple first order finite difference scheme for the discretization of the PBE in a continuous flow vessel. The algorithm introduced could be considered as a special case of the Galerkin method described above where the rectangular rule of integration is used to evaluate the resulting integrals. The resulting discrete set of equations could not be considered consistent with respect to any of the droplet distribution integral properties and so it is expected to converge slowly toward these properties.

The third group of the zero order methods represents an attempt to obtain a set of discrete ODEs from the continuous PBE by forcing these equations to conserve total droplet volume (mass) and number simultaneously. Hounslow et al. (1988) presented a zero discretization approach to discretize the PBE for droplet coalescence and growth by considering all the possible events leading to birth and death of the droplets (particles) in each interval. The discrete population balance appears to conserve correctly the total number of the droplets but not the total droplets volume. To circumvent this problem, the authors introduced a volume correction factor that appears fortunately independent of coalescence frequency function. The major drawback of this approach is in its fixed geometric grid structure and thus making it not amenable to grid refinement. Moreover, Hounslow's approach is not extendable to droplet breakage due to its dependence on the specific nature of the coalescence PBE. Lister et al. (1995) generalized Hounslow's approach to accommodate a variable geometric factor and hence increased its accuracy and flexibility. Kostoglou and Karabelas (1995) discussed several zero order methods for approximating the PBE in the presence of droplet (particle) growth. They concluded that conservative first order finite difference schemes are one of the best choices for problems involving size growth and coagulation (coalescence). Hill and Ng (1995) followed Hounslow's approach to discretize the PBE for droplet breakage by trying to conserve the total droplet number and volume. The major flaw of this approach is its dependence on the form of the breakage frequency and on the type of the grid structure and hence making it impossible to be automated. Vanni (1999) tried to resolve this problem by introducing two correction factors to the discrete set of the PBEs to account for the errors resulting from the intra-interval interactions caused by the overlap of the birth and death events in the same interval or size range (Hill and Ng, 1995; Kumar and Ramkrishna, 1996a). These factors are determined in such a way to conserve the total droplet volume and to correct the death term due to the intra-interval problem. The approach was shown to be less accurate than that of Hill and Ng (1995) by comparing its performance using two simple case studies with known analytical solution. Vanni (2000) had also showed that the combination of this approach for droplet breakage and Lister et al. (1995) approach for droplet coalescence is less accurate than the approach of Kumar and Ramkrishna (1996a). The approach is considered numerically inefficient when compared to the fixed pivot technique due to the double integrals appearing in the discretized PBE. Moreover, the approach does not grantee that the zero moment of the distribution obtained from the discrete set of equations is the same as that obtained from the continuous PBE and hence it is considered internally inconsistent. What we mean by the internal consistency is the following: *the discretized PBE is considered to be internally consistent if any integral property associated with the population density derived from it is exactly the same as that derived from its continuous counterpart* (Ramkrishna, 2000). This specific internal consistency with respect to a certain number of integral properties is shown to improve the accuracy of the predicted droplet distribution and its associated total properties (Hill and Ng, 1995; Kumar and Ramkrishna, 1996a; Attarakih et al., 2003a).

The forgoing brief review of the relevant discretization methods elucidates the practical importance of the zero order methods conserving any two integral properties associated with the droplet distribution and that are independent of the grid structure. We will present in the following section a rigorous mathematical background for the zero order methods of discretization based on the subdomain method (Rice and Do, 1995). This is because all the aforementioned zero-order methods suffer from the lack of a general derivation approach except that introduced by Kronberger (1995).

4. Discretization of the PBE using the subdomain method

The method of weighted residuals has been extensively used in solving the boundary value problems and as a particular case the PBE (Gelbard and Seinfeld, 1978; Kronberger et al., 1995; Nicmanis and Hounslow, 1998; Mahoney and Ramkrishna, 2002). Most of these applications of the weighted residuals use either the Galerkin or the orthogonal collocation methods on finite elements using higher order polynomials of degree three which will not be considered in this work. Since we are concerned in this paper with the zero order methods, the subdomain method as a variation on the theme of weighted residuals will be used. The choice of this method, with the Dirac delta function and the unit step function as the trial and test functions respectively, has a decisive role in eliminating the appearance of the computationally expensive double integrals in the discrete set of the resulting ODEs. However, before we proceed to describe the subdomain method, we have to generalize the PBE given by Eq. (2) to accommodate any quantity of interest, u_m, that is associated with the droplet distribution $n(v,t)$ such as droplet volume for example. This generalization could be done by multiplying both sides of Eq. (2) by u_m and making the necessary transformation to get (Kumar and Ramkrishna, 1996b)

$$\frac{\partial F(v,t)}{\partial t} = \frac{1}{\tau}(F^{\text{feed}}(v,t) - F(v,t)) - \Gamma(v)F(v,t) + \int_v^{v_{\max}} \Gamma(v') \left[\frac{u_m(v)}{u_m(v')}\right] \beta_n(v|v')F(v',t)\,\mathrm{d}v', \quad (7)$$

where $F(v,t)$ is defined as

$$F(v,t) = u_m(v)n(v,t). \tag{8}$$

To project the IPDE given by Eq. (7) into a finite set of ODEs, we discretize the droplet internal coordinate, v, according to the following discrete set: $\{v_{i-1/2}|i=1,\dots M_x+1\}$ with $v_{\min} = v_{1/2} < v_{3/2} < \cdots < v_{M_x+1/2} = v_{\max}$. Let the kth subdomian be defined as $V_k = [v_{k-1/2}, v_{k+1/2})$, $k = 1,\dots M_x$ and the population of the kth subdomian be concentrated at the middle of this subdomain such that $x_k = (v_{k-1/2} + v_{k+1/2})/2$. Then the droplet size distribution is expanded using a point wise sampling of the distribution at the middle of the kth subdomain (also called the pivot) according to the following relation:

$$F^a(v,t) = \sum_{k=1}^{M_x} F_k(t)\delta(v - x_k), \tag{9}$$

where δ refers to the Dirac delta function and the set of the unknown coefficients, $F_k(t)$, refer to the total quantity of droplets in the kth subdomain and are given by

$$F_i(t) = \int_{v_{i-1/2}}^{v_{i+1/2}} u_m(v)n(v,t)\,\mathrm{d}v = u_m(x_i)N_i(t). \tag{10}$$

To proceed further, we choose the test function for the method of weighted residuals as a unit step function in the kth subdomain such that

$$w_k = \begin{cases} 1, & \text{if} \quad v_{k-1/2} \leqslant v < v_{k+1/2} \\ 0, & \text{otherwise.} \end{cases} \tag{11}$$

Now let us define the linear breakage operator as (McGrady and Ziff, 1988):

$$B_o\{v,F(v,t)\} = -\Gamma(v)F(v,t) + \int_v^{v_{\max}} \Gamma(v')\left[\frac{u_m(v)}{u_m(v')}\right] \times \beta_n(v|v')F(v',t)\,\mathrm{d}v'. \tag{12}$$

Accordingly, Eq. (7) could be rewritten as

$$L\{v,F(v,t)\} = \frac{\partial F(v,t)}{\partial t} - \frac{1}{\tau}(F^{\text{feed}}(v,t) - F(v,t)) - B_o(v,F(v,t)) = 0, \tag{13}$$

where we defined $L\{v,F(v,t)\}$ as some differential operator. The right-hand side of Eq. (13) will never be satisfied by substituting $F^a(v,t)$ from Eq. (9) into Eq. (13) since the trial function is only approximation to the exact solution $n(v,t)$. This approximation will result in a nonzero residual that has to be minimized over the whole domain of interest: $v \in [v_{\min}, v_{\max}]$ since the distribution function $n(v,t)$ and so $F(v,t)$ is assumed to vanish for all v outside the interval $[v_{\min}, v_{\max}]$ according to the boundary conditions given by Eqs. (4) and (6). This minimization of the residual is accomplished by multiplying Eq. (13) by the test function, Eq. (11), and integrating the result with respect to v over the interval $[v_{\min}, v_{\max}]$ as follows:

$$\int_{v_{\min}}^{v_{\max}} w_k(v)L\{v,F^a(v,t)\}\,\mathrm{d}v = \sum_{i=1}^{M_x} \int_{v_{i-1/2}}^{v_{i+1/2}} w_k(v)L\{v,F^a(v,t)\}\,\mathrm{d}v = 0. \tag{14}$$

Now, Eq. (14) could be further simplified by substituting Eqs. (11)–(13) into Eq. (14) and after some algebraic manipulation we get

$$\frac{\mathrm{d}F_i(t)}{\mathrm{d}t} = \frac{1}{\tau}(F_i^{feed}(t) - F_i(t)) - \Gamma(x_i)F_i(t) + \sum_{k=i}^{M_x} \Gamma(x_k)F_k(t) \int_{v_{i-1/2}}^{\min(x_k,v_{i+1/2})} \left(\frac{u_m(v)}{u_m(x_k)}\right) \times \beta_n(v|x_k)\,\mathrm{d}v. \tag{15}$$

This equation is exactly the same as that obtained by Kumar and Ramkrishna (1996b) and Ramkrishna (2000) using a completely different approach of derivation (the moving pivot technique for example). Since in many practical situations we are interested in targeting our discrete equations toward the calculation of some total (integral) properties associated with the number density, then it could be shown that the above equation is only consistent with respect to conserving only one such total property. This fact will be shown by first calculating the integral property of the quantity, u_m, from the continuous PBE given by Eq. (7) by integrating its both sides with respect to v over the interval $[v_{\min}, v_{\max}]$ and after some algebraic manipulations one could obtain

$$\frac{\mathrm{d}F(t)}{\mathrm{d}t} = \frac{1}{\tau}(F^{\text{feed}}(t) - F(t)) + \int_{v_{\min}}^{v_{\max}} \Gamma(v')F(v',t)\,\mathrm{d}v' \times \left(\int_0^{v'} \left[\frac{u_m(v)}{u_m(v')}\right] \beta_n(v|v')\,\mathrm{d}v - 1\right), \tag{16}$$

where

$$F(t) = \int_{v_{\min}}^{v_{\max}} u_m(v)n(v,t)\,\mathrm{d}v. \tag{17}$$

Now the right-hand side of Eq. (16) is simplified with the aid of Eq. (9) to

$$\left(\frac{\mathrm{d}F(t)}{\mathrm{d}t}\right)_c = \frac{1}{\tau}(F^{\text{feed}}(t) - F(t))_c + \left(\sum_{i=1}^{M_x} \Gamma(x_i)F(x_i) \times \left[\sum_{k=1}^{i} \int_{v_{k-1/2}}^{\min(x_i,v_{k+1/2})} \left(\frac{u_m(v)}{u_m(x_i)}\right) \beta_n(v|x_i)\,\mathrm{d}v - 1\right]\right)_c, \tag{18}$$

where the c subscript on both sides indicates that the time change of the integral property that is derived from the continuous PBE to differentiate it from the discrete one (with subscript d). On the other hand, the time change of the integral property as derived from the discrete PBE could be obtained by summing Eq. (15) i from 1 to M_x:

$$\left(\frac{\mathrm{d}F(t)}{\mathrm{d}t}\right)_d = \frac{1}{\tau}(F^{\mathrm{feed}}(t) - F(t))_d + \left(\sum_{i=1}^{M_x} \Gamma(x_i)F(x_i) \times \left[\sum_{k=1}^{i} \int_{v_{k-1/2}}^{\min(x_i, v_{k+1/2})} \left(\frac{u_m(v)}{u_m(x_i)}\right) \beta_n(v|x_i)\,\mathrm{d}v - 1\right]\right)_d. \quad (19)$$

It is clear that the last two equations are exactly identical and hence the discrete PBE given by Eq. (15) is internally consistent with respect to any single integral property. For example if $u_m(v) = 1$, we get a single ODE describing the evolution of the total number concentration, $N(t)$. On the other hand, if $u_m(v) = v$, the term between the squared brackets is zero due to the conservation of total droplet volume, and hence we end up with the rate of change of the dispersed phase hold up (concentration) due to the in and out flows across the vessel boundaries.

Now, to gain more insight into the problem of integral property conservation, we let $u_m = 1$ in Eq. (15) and we will call the resulting set of discrete equations as the base discrete set. This could be justified since all the other discrete integral properties are derived from these base equations by multiplying it with $u_m(x_i)$. So, the base discrete set of ODEs follows from Eq. (15)

$$\frac{\mathrm{d}N_i(t)}{\mathrm{d}t} = \frac{1}{\tau}(N_i^{\mathrm{feed}}(t) - N_i(t)) - \Gamma(x_i)N_i(t) + \sum_{k=i}^{M_x} \Gamma(x_k)N_k(t) \int_{v_{i-1/2}}^{\min(x_k, v_{i+1/2})} \beta_n(v|x_k)\,\mathrm{d}v. \quad (20)$$

As stated previously, this equation is consistent only with respect to the total number of concentration according to Eq. (18) and Eq. (19). If the prediction of the other discrete integral properties is demanded, then it could be obtained from this equation by multiplying its both sides by $u_m(x_i)$ and denoting $u_m(x_i)N_i\ (t) = (F_i(t))_d$ to differentiate it from the continuous integral property: $(F_i(t))_c$ obtainable from Eq. (15)

$$\left(\frac{\mathrm{d}F_i(t)}{\mathrm{d}t}\right)_d = \frac{1}{\tau}(F_i^{\mathrm{feed}}(t) - F_i(t))_d - \left(\Gamma(x_i)F_i(t) - \sum_{k=i}^{M_x} \Gamma(x_k)F_k(t) \left(\frac{u_m(x_i)}{u_m(x_k)}\right) \int_{v_{i-1/2}}^{\min(x_k, v_{i+1/2})} \beta_n(v|x_k)\,\mathrm{d}v\right)_d \quad (21)$$

and by summing both sides of this equation over i from 1 to M_x we get

$$\left(\frac{\mathrm{d}F(t)}{\mathrm{d}t}\right)_d = \frac{1}{\tau}\left(F^{\mathrm{feed}}(t) - F(t)\right)_d + \left(\sum_{i=1}^{M_x} \Gamma(x_i)F(x_i) \left[\sum_{k=1}^{i} \left(\frac{u_m(x_k)}{u_m(x_i)}\right) \int_{v_{k-1/2}}^{\min(x_i, v_{k+1/2})} \beta_n(v|x_i)\,\mathrm{d}v - 1\right]\right)_d. \quad (22)$$

It is clear now that Eq. (22) is only identical to Eq. (18) if $(F^{\mathrm{feed}}(x_i))_d = \int_{v_{i-1/2}}^{v_{i+1/2}} u_m(v)n^{\mathrm{feed}}(v)\,\mathrm{d}v$ and $u_m(v) = 1$; that is the internal consistency is only recovered for the base set of the discrete equations as expected. Actually, we can only recover the internal consistency with respect to any integral property in the case of very fine grids such that the mean value theorem of integrals is valid so that Eq. (18) and Eq. (22) are identical. Unfortunately, since the daughter droplet distribution becomes sharp and narrow in the small size range (as x_k becomes small), then the integrand on the right-hand side of Eq. (18) becomes also sharp and depending on the variation of $u_m(v)$, hence calling for very fine grid. Since our aim is to make use of the less computationally expensive coarse grid, we have to seek another approach to recover the internal consistency of Eq. (21) at least with respect to some specific integral properties rather than all of them. To do so, we will first briefly introduce the fixed-pivot technique of Kumar and Ramkrishna (1996a) before we lay down our approach for the purpose of comparison since they are closely interrelated.

5. The fixed-pivot technique

We start by considering the formation term in the PBE given by Eq. (2) and let us consider a daughter droplet of volume v resulting from the breakage of a mother droplet of volume v'. Since the droplet volume coordinate is discretized into a finite number of subdomains, then it is only allowed for droplet of sizes, x_k, to be represented in the kth subdomain during the transformation from the continuous to the discrete domains. If the resulting daughter droplet volume, v, does not coincide with any of the available representative sizes (pivots) of the subdomains, then the simplest way to do it is to assign it to the nearest representative size. This type of assignment could only preserve one integral property in the discrete form as we have shown in the previous section. The genius idea of the fixed pivot technique is to redistribute the property of the formed droplet

between two adjacent subdomains, V_{k-1} and V_k, at their representative sizes, x_{k-1}, and x_k, provided that $v \in [x_{k-1}, x_k)$ such that any two integral properties are enforced due to the transformation from the continuous to the discrete domains. Kumar and Ramkrishna (1996a) showed that for the conservation of any two properties, $u_1(v)$, and $u_2(v)$, we could set up the following two constraints by assigning the fractions $\gamma_{k-1}^{<k-1>}(v)$ and $\gamma_k^{<k-1>}(v)$ to the droplet populations at x_{k-1} and x_k respectively:

$$\gamma_{k-1}^{<k-1)}(v)u_m(x_{k-1}) + \gamma_k^{<k-1>}(v)u_m(x_k) = u_m(v), \quad m = 1, 2, \tag{23}$$

where the fractions $\gamma_{k-1}^{<k>}(v)$ and $\gamma_k^{<k>}(v)$ are found by solving the linear system given by Eq. (23). Note that the subscript in the previous fractions refers to the representative size while the superscript refers to the representative size range. It is obvious from these constraints that droplet population in the kth subdomain receives a net gain of droplet population for every daughter droplet that is formed in the range $[x_{k-1}, x_{k+1}]$. This calls for the modification of the formation term appearing in Eq. (12) (for more details see Kumar and Ramkrishna, 1996a).

Proceeding as we have done in the previous section, the final base set of the discrete equations is given by

$$\frac{\mathrm{d}N_i(t)}{\mathrm{d}t} = \frac{1}{\tau}(N_i^{\mathrm{feed}}(t) - N_i(t)) - \Gamma(x_i)N_i(t) + \sum_{k=i}^{M_x} \pi_{i,k}^{<m>}\Gamma(x_k)N_k(t), \tag{24}$$

where the breakage matrix elements $\pi_{i,k}^{<m>}$ could be written as

$$\pi_{i,k}^{<m>} = \int_{x_{i-1}}^{x_i} \gamma_i^{<i-1>}(v)\beta_n(v|x_k)\,\mathrm{d}v + \int_{x_i}^{\min(x_k, x_{i+1})} \gamma_i^{<i>}(v)\beta_n(v|x_k)\,\mathrm{d}v \tag{25}$$

The upper limit of the integration on the second integral is introduced to take into account the fact that the daughter droplet volume, v, cannot exceed its mother droplet volume, x_k. The discrete set of equations given by Eq. (24) is *approximately* internally consistent with respect to any two integral properties as shown by Ramkrishna (2000). However, in their original work Kumar and Ramkrishna (1996a) set the first integral to zero for $i = 1$ since the representative size (pivot) x_0 does not exist. Since x_1 is greater than zero, it follows that any droplet having volume less than x_1 will be lost from the left boundary. This loss becomes significant for large residence time or batch time for continuous and batch systems, respectively. This error will be called the IDE and will be quantified in the next section.

6. The IDE of the fixed-pivot technique

It is clear that the present fixed-pivot technique could not exactly conserve the prescribed integral properties exactly due to the IDE; but instead it conserves one of them approximately. The reason for this approximation is clear if we reconsider the system of linear equations given by Eq. (23) for $k = 1$, and let us concentrate on the conservation of total droplet number concentration and the fractional volume of the dispersed phase (hold up). Since the representative droplet volume x_0 does not exist we have two equations in one unknown; namely $\gamma_1^{<0>}(v) = 1$ and $\gamma_1^{<0>}(v)x_1 = v$. This means that any daughter droplet that is born in the size range $[v_{\min}, x_1)$ will be totally assigned to the representative droplet size x_1 indicating that only the total droplet number concentration is exactly conserved. This inherent error associated with the fixed-pivot technique is really unavoidable and it causes a loss of the second integral property from the left boundary if the first integral property is to be exactly conserved particularly if x_1 is not sufficiently small. Since the dispersed phase hold up, ϕ, should be exactly conserved, we will pay a particular attention to this integral quantity, and the other one will be chosen as the number concentration, $N(t)$. Doing so, we are ready to derive a quantitative measure of this IDE through multiplying Eq. (24) by x_i and summing both sides over $i = 1$ to M_x and after some algebraic manipulation it is not difficult to show

$$\tau\frac{\mathrm{d}\phi(t)}{\mathrm{d}t} = (\phi^{\mathrm{feed}}(t) - \phi(t)) - \tau\sum_{k=1}^{M_x}\Gamma(x_k)N_k(t)\int_0^{x_1}(v - x_1)\beta_n(v|x_k)\,\mathrm{d}v. \tag{26}$$

It is the second term on the right-hand side that we termed the IDE, and it is clear that it is proportional to the magnitude of the first representative size and will never tend to zero since x_1 is always greater than zero. It is also worthwhile to note that the IDE has a cumulative nature and is increasing with time since the set $\{N_i(t)|i = 1, \ldots i_{\max}\}$ is an increasing set of functions, where $i_{\max}$ is some index above which discrete population densities are decreasing with time. This maximum index always exists due to the loss and formation terms comprising the linear breakage operator. This is because the subdomains of the upper size range start to loss their population while the small size range subdomains receive a net gain of the droplet population. So, if the total number of droplets is approximately conserved, then the error in the first moment of the distribution will be much larger (Attarakih et al., 2003a).

Note that at steady state the IDE could be accurately estimated from Eq. (26) according to the following relation

$$IDE(x_1) = \tau\sum_{k=1}^{M_x}\Gamma(x_k)N_k(t=\infty)\int_0^{x_1}|(v - x_1)|\beta_n(v|x_k)\,\mathrm{d}v = |\phi^{\mathrm{feed}} - \phi(t=\infty)|. \tag{27}$$

Now, the second term on the right-hand side of this equation could be identically zero if the total volume concentration is exactly conserved. So, the magnitude of deviation of this term from zero represents an indirect estimation of the IDE since the feed hold up, ϕ^{feed} is exactly known.

7. The present discretization approach

It should be first emphasized that the recovery of internal consistency (as pointed out in Section 4) with respect to certain integral properties is not necessarily corresponding to the same number distribution function. This means that we could estimate for example one integral property from two number distributions that are slightly different. For example, one such integral property is the total number concentration (the zero moment of the distribution) corresponding to the total area under the number density curve. Now, we could generate an infinite number of these number density curves but still having the same total area. By referring to Section 4 and particularly to Eqs. (18) and (22) it has been shown that there exists only one degree of freedom to make these two equations identical. The question arises at this stage is how we could increase the degrees of freedom to two such that any two integral properties associated with the base set of equations could be achieved? This question might be answered by taking into consideration the aforementioned discussion concerning the non-uniqueness of the number density function (and hence the base set of equations) from which the integral properties are derived. It then appears that it is feasible to solve a modified but slightly different PBE with the property that the base set of equations of this slightly modified PBE is internally consistent with respect to any two integral properties. However, this does not mean that the slightly modified PBE will converge to a completely different or erroneous number distribution. This is because we enforce the slightly modified PBE to be identical to its original counterpart at least with respect to the desired integral properties. It should also be stressed that the discrete solution generated by the base set of equations of this slightly modified PBE should converge to the solution of its continuous counterpart as the grid is made fine.

To proceed further, we introduce the pair of auxiliary functions: $\eta(v)$ and $\sigma(v)$ to account for the intra-interval problem when the PBE is transformed from the continuous to the discrete domains. So, the proper choice of placing these functions is at the loss and formation terms so that we could obtain the following modified linear breakage operator:

$$B_o\{v,F(v,t)\} = -\eta(v)\Gamma(v)F(v,t) + \int_v^{v_{\max}} \sigma(v')\Gamma(v') \times \left[\frac{u_m(v)}{u_m(v')}\right] \beta_n(v|v')F(v',t)\,\mathrm{d}v'. \quad (28)$$

Now substituting this expression in Eq. (13) and making use of Eq. (11), and Eq. (14) and by setting $u_m(v) = 1$, the following modified base set of equations is obtained

$$\frac{\mathrm{d}N_i(t)}{\mathrm{d}t} = \frac{1}{\tau}(N_i^{\text{feed}}(t) - N_i(t)) - \eta(x_i)\Gamma(x_i)N_i(t) + \sum_{k=i}^{M_x} \sigma(x_k)\Gamma(x_k)N_k(t) \times \int_{v_{i-1/2}}^{\min(x_k,v_{i+1/2})} \beta_n(v|x_k)\,\mathrm{d}v. \quad (29)$$

Before we proceed further to determine the forms of the introduced functions $\eta(x_i)$ and $\sigma(x_i)$ we have to generalize Eq. (29) to handle any discrete property, $u_m(x_i)$ exactly in the same way as we did in obtaining Eq. (21):

$$\left(\frac{\mathrm{d}F_i(t)}{\mathrm{d}t}\right)_d = \frac{1}{\tau}(F_i^{\text{feed}}(t) - F_i(t))_d - \left(\eta(x_i)\Gamma(x_i)F_i(t) - \sum_{k=i}^{M_x} \sigma(x_k)\Gamma(x_k)F_k(t)\left(\frac{u_m(x_i)}{u_m(x_k)}\right) \times \int_{v_{i-1/2}}^{\min(x_k,v_{i+1/2})} \beta_n(v|x_k)\,\mathrm{d}v\right)_d \quad (30)$$

and by summing both side of this equation over i from 1 to M_x we get

$$\left(\frac{\mathrm{d}F(t)}{\mathrm{d}t}\right)_d = \frac{1}{\tau}(F^{\text{feed}}(t) - F(t))_d + \left(\sum_{i=1}^{M_x} \Gamma(x_i)F(x_i) \times \left[\sigma(x_i)\sum_{k=1}^{i}\left(\frac{u_m(x_k)}{u_m(x_i)}\right) \times \int_{v_{k-1/2}}^{\min(x_i,v_{k+1/2})} \beta_n(v|x_i)\,\mathrm{d}v - \eta(x_i)\right]\right)_d. \quad (31)$$

Now we are ready to determine the form of the discrete functions $\eta(x_i)$ and $\sigma(x_i)$ by enforcing internal consistency of Eq. (30) with respect to any two integral properties that are associated with the number distribution. This could be simply accomplished by equating the right-hand sides of Eq. (18) and Eq. (31) to get the following two set of constraints:

$$(F^{\text{feed}}(x_i))_d = \int_{v_{i-1/2}}^{v_{i+1/2}} u_m(v)n^{\text{feed}}(v)\,\mathrm{d}v, \quad (32)$$

$$\sigma(x_i)\sum_{k=1}^{i}\left(\frac{u_m(x_k)}{u_m(x_i)}\right)\int_{v_{k-1/2}}^{\min(x_i,v_{k+1/2})} \beta_n(v|x_i)\,\mathrm{d}v - \eta(x_i) = \sum_{k=1}^{i}\int_{v_{k-1/2}}^{\min(x_i,v_{k+1/2})}\left(\frac{u_m(v)}{u_m(x_i)}\right) \times \beta_n(v|x_i)\,\mathrm{d}v - 1, \quad m = 1,2. \quad (33)$$

The first constraint given by Eq. (32) is imposed due to the droplet transport across the system boundary along with the feed. The second set of constraints is due to the internal inconsistent resulting from the discrepancy between the continuous and discrete nature of the droplet breakage. These constraints form a system of two linear equations in $\eta(x_i)$ and $\sigma(x_i)$ that are linearly independent for all values of $i = 2,\dots M_x$. However, for $i = 1$ there is only one independent equation as we will show in the next section. The solution of this system of equations could be written in the following form for any two desired integral properties $u_1(v)$ and $u_2(v)$:

$$\sigma(x_i) = \frac{q_2(x_i) - q_1(x_i)}{r_2(x_i) - r_1(x_i)}, \tag{34}$$

$$\eta(x_i) = 1 + [\sigma(x_i) r_2(x_i) - q_2(x_i)], \tag{35}$$

where

$$r_m(x_i) = \sum_{k=1}^{i} \left(\frac{u_m(x_k)}{u_m(x_i)}\right) \int_{v_{k-1/2}}^{\min(x_i, v_{k+1/2})} \beta_n(v|x_i)\,\mathrm{d}v,$$

$$m = 1, 2, \tag{36}$$

$$q_m(x_i) = \sum_{k=1}^{i} \int_{v_{k-1/2}}^{\min(x_i, v_{k+1/2})} \left(\frac{u_m(v)}{u_m(x_i)}\right) \beta_n(v|x_i)\,\mathrm{d}v,$$

$$m = 1, 2, \tag{37}$$

for $i = 2,\dots,M_x$ and $\eta(x_i) = \sigma(x_i) = 1$ for $i = 1$.

For a especial case of conserving droplet number and volume concentrations, the above equations could be simplified by setting $u_1(v) = 1$ and $u_2(v) = v$ to get:

$$\sigma(x_i) = \frac{\vartheta(x_i) - 1}{\vartheta(x_i) - r_2(x_i)}, \tag{38}$$

$$\eta(x_i) = \sigma(x_i) r_2(x_i), \tag{39}$$

$$r_2(x_i) = \sum_{k=1}^{i} \left(\frac{x_k}{x_i}\right) \int_{v_{k-1/2}}^{\min(x_i, v_{k+1/2})} \beta_n(v|x_i)\,\mathrm{d}v, \tag{40}$$

where $\vartheta(x_i)$ is the average number of daughter droplets produced by breakage.

Since $\vartheta(x_i) \geqslant 2$ and $(x_k/x_i) \leqslant 1$ for $k = 1,\dots,i$, it is then not difficult to show that $\vartheta(x_i) \geqslant r_2(x_i)$. The equality sign holds only for $k = i = 1$ where the system of equations (37) losses its linear independency, and hence $\eta(x_i) = \sigma(x_i) = 1$. This means that the auxiliary functions $\eta(x_i)$ and $\sigma(x_i)$ given by Eqs. (39) and (40) are always positive as required.

It is clear that the modified base set of equations given by Eq. (29) and the two auxiliary functions $\eta(x_i)$ and $\sigma(x_i)$ given by Eqs. (35) and (36) are free from any assumption concerning the droplet breakage functions or the type of grid. This makes these equations cope, in a flexible way, with binary or multiple droplet breakage in a straightforward manner. This approach also allows a combination of different types of grids (e.g. linear, geometric, ... etc.) even for a single problem and does make grid refinement a possible way to improve the numerical accuracy whenever it is required. Moreover, the generality of the conservation of any two desired integral properties makes the approach attractive for directing the calculations toward the targeted dispersed phase quantities that are of practical interest (such as hold up, $d32,\dots$ etc.). In addition, the internal consistency of the approach makes it easy to be coupled with the fixed-pivot technique of Kumar and Ramkrishna (1996a) for droplet coalescence.

It should be noted that the correction factors introduced by Hill and Ng (1995) and Vanni (1999) to the discrete PBE for droplet breakage were an attempt to obtain discrete functions like $\eta(x_i)$ and $\sigma(x_i)$. However, the main concern of the first author is to conserve only the total number and volume concentrations that are only applicable to special limited cases of breakage functions. The second author tried to resolve this problem by introducing a correction factor for the loss term without guarantee to produce an internal consistency with respect to the total droplet concentration.

8. The IDE of the present discretization approach

As in the case of the fixed-pivot technique, the present discretization approach could not exactly conserve the prescribed integral properties exactly due to the IDE; but instead it conserves one of them approximately. The reason for this approximation is the loss of linear dependency in the first subdomain. For this case we choose as in the case of the fixed-pivot technique to conserve the total number concentration, $N(t)$, and leave the total volume concentration, $\phi(t)$, approximately conserved. This could be done by setting $\eta(x_i) = \sigma(x_i) = 1$ for $i = 1$ and $u_2(v) = v$ and noting that the term between the square brackets is identically zero except for $i = 1$ due to the constraints given by Eqs. (34) and (35). So, Eq. (31) simplifies to

$$\tau \frac{\mathrm{d}\phi(t)}{\mathrm{d}t} = (\phi^{\mathrm{feed}}(t) - \phi(t)) + \tau x_1 \Gamma(x_1) N(x_1)(\vartheta(x_1) - 1). \tag{41}$$

As stated previously the second term on the right-hand side is the IDE and it is clear that it is proportional to the magnitude of the first representative droplet size and will never tend to zero if $\Gamma(x_1)$ and $N(x_1) > 0$ since x_1 is always greater than zero.

Note that at steady state the IDE could be accurately estimated from Eq. (41) according to the following relation:

$$\mathrm{IDE}(x_1) = \tau x_1 \Gamma(x_1)(\vartheta(x_1) - 1) N_1(t = \infty) = |\phi^{\mathrm{feed}} - \phi(t = \infty)|. \tag{42}$$

From this result, it is worthwhile to note that the magnitude of the IDE of the present approach is much smaller than that of the fixed-pivot technique given by Eq. (27) and

has not a cumulative nature. This is not surprising since the present discretization approach does not redistribute the resulting droplet volume due to any breakage event between two contiguous subdomains as the fixed-pivot does. So, to this redistribution we attribute the cumulative nature of the IDE of the fixed-pivot technique. However, in the present approach the formation and loss terms adjust themselves automatically in each subdomain to conserve the desired integral properties through the aid of the auxiliary functions $\eta(x_i)$ and $\sigma(x_i)$. Moreover, if the representative droplet size, x_1, is chosen to be less than $v_{\min}$, then the IDE of the present approach is identically zero due to the regulatory condition given by Eq. (6). So, it could be concluded that the present discretization approach is superior to the fixed-pivot technique at least from the IDE point of view.

9. Validation and realization of the present discretization approach

In this work, the numerical accuracy and convergence for the present discretization approach and the fixed-pivot technique were tested using two classes of case studies. The first class is merely of theoretical form were analytical solutions are possible, while the second class belongs to real interacting liquid–liquid dispersions without known analytical solutions.

Since droplet diameter is practically used as the droplet internal coordinate, it is desirable to transform the volume internal coordinate in the final discrete PBEs given by Eq. (24) and Eq. (29) and the other related equations. As stated previously, the transformation of coordinate is easier when the PBE in discrete form rather than in the continuous form by making use of the following identity:

$$\int_{v_{i-1/2}}^{v_{i+1/2}} n(v,t)\,\mathrm{d}v = \int_{d_{i-1/2}}^{d_{i+1/2}} n(d,t)\partial d \tag{43}$$

and hence, $N(x_i)=N(d_i)$. If the transformation of coordinate occurs without integration, then the following relation must be used:

$$n(d,t) = \frac{\partial v}{\partial d}\, n(v,t). \tag{44}$$

The above two relations are sufficient to transform the discrete PBEs from volume to diameter coordinate. It should also be clarified that the integrals appearing in Eqs. (25), (32) and (40) are estimated numerically using a 5-point Gauss quadrature. Additionally, in all the simulations performed in this work, the droplet diameter is discretized according to the following geometric grid:

$$d_{k+1/2} = \left(\frac{d_{\max}}{d_{\min}}\right)^{k/M_x} d_{\min}, \quad k = 0,\ldots,M_x. \tag{45}$$

The system of ODEs given by either Eq. (24) or Eq. (29) are integrated using the implicit Euler method with a constant time step. Although the method is of first order accuracy it has two distinct advantages: the first one is its stability that is independent of the size of the time step, and the second is the guarantee that the resulting solution is always positive, which is a requirement imposed by the physical process itself. The algorithm presents itself as an efficient scheme especially when the PBE is extended to model the dispersed phase in multistage or differential flow systems (countercurrent liquid–liquid extraction columns) (Attarakih et al., 2003b, 2004).

9.1. Validation of the present discretization approach

In this validation phase we have chosen the set of functions and parameters shown in Table 1 for the present breakage problem (cases 1 and 2). To the best of the authors' knowledge, the PBE given by Eq. (2) has no general analytical solution. However, McGrady and Ziff (1988) proposed an analytical solution for a slightly different form of Eq. (2) and a special case of monodisperse feed distribution. Nicmanis and Hounslow (1998) proposed an analytical solution only for the steady state version of the breakage problem given by Eq. (2) using the conditions for case 1. So, we provide in this work the following analytical solutions of Eq. (2) for cases 1 and 2 as a sum of transient and steady state solutions, where the detailed derivation is listed in Appendix A

$$n(d,t) = \frac{3d^2 N_0^f}{d_0^3}\left[n_t(d,t) + n(d,\infty)\right] \tag{46}$$

for $p = 1$ (see Table 1) we have

$$n_t(d,t) = -\left\{\frac{t^2}{a} + \left(2\tau\left[1+\frac{t}{\tau_b}\right]\left[\frac{1}{a^2}+\frac{\tau}{a^3}\right]+\frac{1}{a}\right)\right\} \times \mathrm{e}^{-(d/d_0)^3 - t/\tau_b}, \tag{47}$$

$$n(d,\infty) = \left(\frac{1}{a} + \frac{2\tau}{a^2} + \frac{2\tau^3}{a^3}\right)\mathrm{e}^{-(d/d_0)^3} \tag{48}$$

and for $p = 2$ (see Table 1) we have

$$n_t(d,t) = \left\{a\left(\frac{t}{\tau_b}\right) - \left(1+\frac{t}{\tau_b}\right)\left(1+\tau + \tau\left[1+\left(\frac{d}{d_0}\right)^3\right]^2\right)\right\}\frac{\mathrm{e}^{-(d/d_0)^3-(t/\tau_b)}}{a^2}, \tag{49}$$

$$n(d,\infty) = \left(1+\tau+\tau\left[1+\left(\frac{d}{d_0}\right)^3\right]^2\right)\frac{\mathrm{e}^{-(d/d_0)^3}}{a^2}, \tag{50}$$

Table 1
Case studies for the validation and realization of the present discretization approach

Case	$n^{\text{feed}}(d)$	$n(d,0)$	$\beta_n(d\|d')$	$\Gamma(d)$
1	$\frac{3d^2N_0^f}{d_0^3}\,\mathrm{e}^{-(d/d_0)^3}$	zero	$6\,\frac{d^2}{d'^3}$	$\left(\frac{\pi d^3}{6}\right)^p,\ p=1$
2	The same as case 1	zero	The same as case 1	The same as case 1 with $p=2$
3	Log-normal	zero	$\frac{90\vartheta d^2}{d'^3}\left(\frac{d}{d'}\right)^6\left(1-\left[\frac{d}{d'}\right]^3\right)^2$ Alopaeus et al. (1999)	$C_1\,\frac{\varepsilon^{1/3}}{(1+\phi)d^{2/3}}\,\mathrm{e}^{(-C_2(\sigma(1+\phi)^2/(\rho_d\varepsilon^{3/2}d^{5/3}))}$, $C_1=0.00481,\ C_2=0.08$ Coulaloglou and Tavlarides (1977).
4	Log-normal	zero	$\frac{3c\vartheta}{\sqrt{2\pi}}\left(\frac{d^2}{d'^3}\right)\mathrm{e}^{-((c^2/2)[1-\vartheta(d/d')^3]^2)}$ $c=3.5$ Coulaloglou and Tavlarides (1977).	$C_3\varepsilon^{1/3}\mathrm{erfc}\left(\sqrt{C_4\,\frac{\sigma}{\rho_c\varepsilon^{2/3}d^{5/3}}+C_5\,\frac{\mu_d}{d^{4/3}\varepsilon^{1/3}\sqrt{\rho_c\rho_d}}}\right)$ $C_3=0.986\ \mathrm{m}^{-2/3}$, $C_4=0.892\times10^{-3}$ and $C_5=0.2$ Alopaeus et al. (2002).

$$\tau_b=\frac{\tau}{1+\tau\left(\frac{d}{d_0}\right)^{3p}},\quad p=1,2, \tag{51}$$

$$a=1+\tau\left(\frac{d}{d_0}\right)^{3p},\quad p=1,2. \tag{52}$$

It should be noted that Eq. (46) is reduced exactly to that derived by Nicmanis and Hounslow (1998) at steady state. The most important fact that could be drawn from Eq. (51) that the breakage time constants are dependent as expected on the breakage frequency. Moreover, the breakage time constant, τ_b, in a perfectly mixed vessel is always less than the vessel time constant, τ. These time constants are dependent only on the droplet diameter and the vessel time constant, thus small droplets exhibit longer breakage times than the larger ones.

All the numerical studies that will be presented for these two case studies are based on conserving droplet volume and number; that is $u_1t(v)=1$ and $u_2(v)=v$. It should also be clear that the geometric grid given by Eq. (45) is constructed with number of subdomains (or pivots) $M_x=50$ unless it is stated for some particular cases. The magnitude of the time step, Δt, was chosen to trade off between the computational accuracy and the execution time. A value of $\Delta t=1$ s was found satisfactory for all the numerical tests. The droplet distribution is solved for in terms of the droplet volume concentration by multiplying Eq. (24) by $v(d_i)$ for the fixed-pivot technique, while we set $u_m(v)=v$ in Eq. (30) for the present discretization approach and substituting $\varphi_i(t)=v(d_i)N_i(t)$. The droplet volume density is then recovered from the droplet volume concentration using the following relation:

$$P(d_i,t)=\frac{\varphi(d_i,t)}{\sum_{i=1}^{M_x}\varphi(d_i,t)\Delta d_i},\quad i=1,\ldots,M_x, \tag{53}$$

while the analytical volume density $p(d,t)$ is obtained from Eq. (46) through Eq. (52) using a continuous analog of Eq. (53) with a very fine uniform grid of 1000 intervals. The main advantage of using the volume instead of the number density may be justified by obtaining the dispersed phase hold up directly by summing the local hold up of each class ($\phi(t)=\sum_{i=1}^{M_x}\varphi(d_i,t)$) (Ribeiro et al., 1995; Alopaeus et al., 2002). The numerical moments of the distribution are calculated based on the discrete number concentration, $N(d_i,t)$ according to the following relation:

$$M_j(t)=\sum_{i=1}^{M_x}d_i^jN(d_i,t),\quad j=0,1,\ldots\ . \tag{54}$$

Similarly, the exact moments are calculated from a continuous analog to the previous equations except when $j=0$ and 3 where simple explicit forms are available (Attarakih et al., 2003a).

To completely define the problem at hand, the dispersed feed hold up is specified ($\phi^{\text{feed}}=0.4$) for cases 3 and 4, where this relatively high value of the hold up seems to contradict the assumption of negligible droplet coalescence. The reason for this value is just only to be consistent with the experimentally validated breakage functions at this value of hold up (Alopaeus et al., 2002). Anyhow, we think from numerical point of view that the discretization approach should be applicable for a wide range of the dispersed phase hold up.

It should also be noted that in all the figures in this work we denoted the present discretization approach by: present approach and the generalized fixed pivot by GFP. Moreover, in all the case studies below, the minimum and maximum droplet diameters were chosen so that the total number and volume of the droplets reporting outside this range is less than 0.1% until the steady state is reached. This is termed the total finite domain error and is dealt with in detail by Attarakih et al. (2004).

9.1.1. Case 1: $\Gamma(d)=\pi d^3/6$

In this case the droplet breakage frequency is considered to be proportional to the droplet volume. We start our presentation of the numerical results by shedding some light

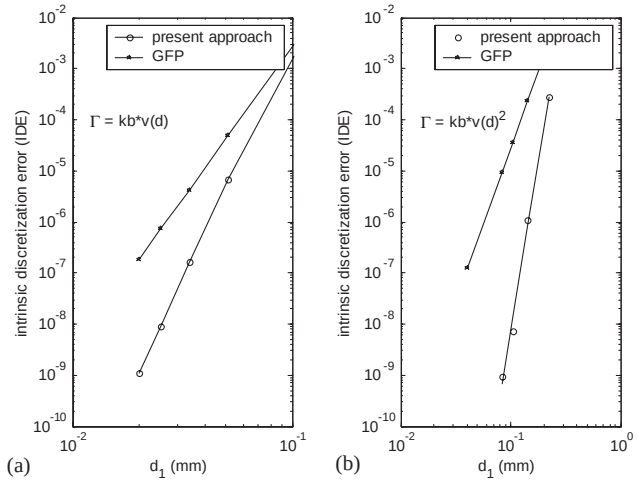

Fig. 1. The steady state intrinsic discretization error (IDE) using the present approach and the GFP technique: (a) $\Gamma(d) = k_b(\pi d^3/6)$, (b) $\Gamma(d) = k_b(\pi d^3/6)^2$ where $k_b = 1$, $\tau = 100$ s, and the inlet feed distribution is given by Eq. (50) with $d_0 = 1$ and $N_0^f = 1$.

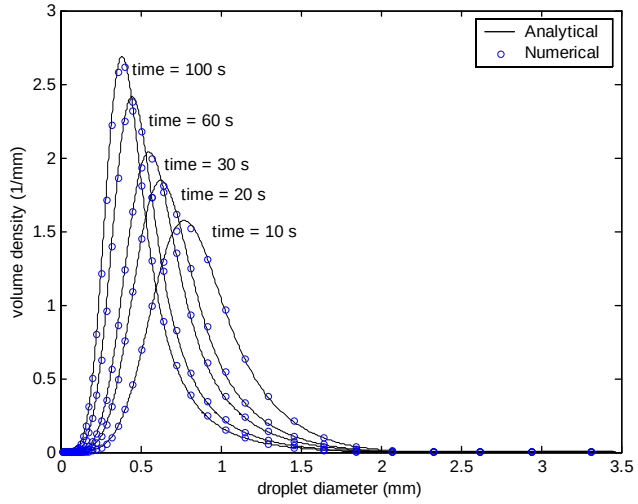

Fig. 2. The dynamic evolution of the droplet volume density: $\Gamma(d) = k_b(\pi d^3/6)$ with $k_b = 1$, $\tau = 100$ s, and $M_x = 50$.

on the behavior of the intrinsic discretization error (IDE) of both the present discretization approach and the generalized fixed-pivot technique (GFP). Fig. 1a depicts the variation of the IDE at steady state based on the relations given by Eqs. (27) and Eq. (42) for the GFP and the present discretization approach respectively. First, the present approach has a smaller IDE than that of the GFP as is predicted by Eqs. (27) and (42). Second, the variation of the IDE as a function of the droplet diameter in the first subdomain (d_1) seems to be linear on a log-log plot, which may be attributed to the power law breakage frequency.

Fig. 2 shows the dynamic evolution of the volume density at different times over a one-time constant period where the changes in the droplet population are evidently sharp. The minimum and maximum droplet diameters were chosen as $d_{\min} = 0.001$ and $d_{\max} = 3.5$ mm. Also, the minimum droplet diameter is sufficiently small to make the IDE of negligible value particularly for sufficient number of subdomains ($Mx = 50$) as it is clear from Fig. 2a. For the sake of clarity, the predicted solution using the GFP is not shown along with the present approach on this figure since the two solutions are almost identical. This is really not surprising, since the two approaches are based on the same framework of conserving any two integral properties associated with the distribution. It is clear also that there is a close match between the analytical solution obtained from Eqs. (46) through (48) and the numerical solution at all times. Note that the dynamic evolution of the droplet population in the small size range is sharper than that at the large size range due to the differences in the breakage time constants ($[\tau_b]_{\text{small droplets}} > [\tau_b]_{\text{large droplets}}$) as predicted by Eq. (51). It is also worthwhile to mention here that due to the geometric grid used in the discretization, numerical errors are likely to appear on the upper tail of the distribution. This error is attributed to the increasing size of the subdomains and hence increasing the integration error with respect to d. This error could be reduced through either increasing the number of subdomains or by refining the grid on the upper size range (Kumar and Ramkrishna, 1996a), where the former one is adopted here ($M_x = 50$). The steady state solution for this case is also shown in Fig. 8a where again the agreement between the numerical and analytical solutions is excellent.

9.1.2. Case 2: $\Gamma(d) = (\pi d^3/6)^2$

In this case the droplet breakage frequency is proportional to the square of the droplet volume. This case is somewhat different from case 1 from the dynamic and steady state point of view. This is clear if we focus again on the breakage time constant given by Eq. (51) with $p = 2$. This time constant indicates that droplets having volume less than one show slower dynamics when they are compared to those having the same volume in case 1. On the other hand, droplets having volume greater than one exhibit faster dynamics as compared with those in case 1. Due to this it is expected to have slow dynamics at the small size range for the droplet breakage as the steady state is approached when compared to case 1. Moreover, due to the fast and slow breakage rates for the small and large sizes respectively, it is expected to have a sharp transition in the droplet distribution through passing from droplets having $v > 1$ to those with $v < 1$, where these facts are clear if we compare both breakage rates for $p = 1$ and 2 as they are depicted in Fig. 4. It is clear from this figure that the breakage rate of case 2 is only greater than that of case 1 for droplet diameter greater than 1.5 mm approximately. Fig. 5 shows the predicted and the analytical solutions as obtained from Eqs. (49)–(52) with $p = 2$, where the two solutions are almost identical. The predicted solution using the present approach is obtained

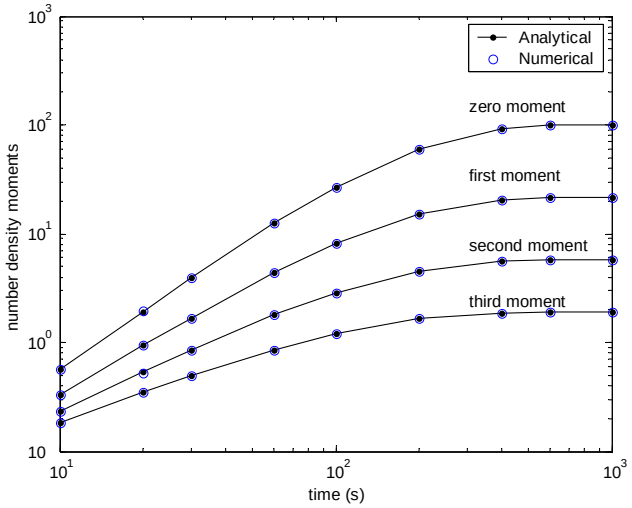

Fig. 3. The dynamic evolution of the number density moments: $\Gamma(d) = k_b(\pi d^3/6)$ with $k_b = 1$, $\tau = 100$ s, and $M_x = 50$.

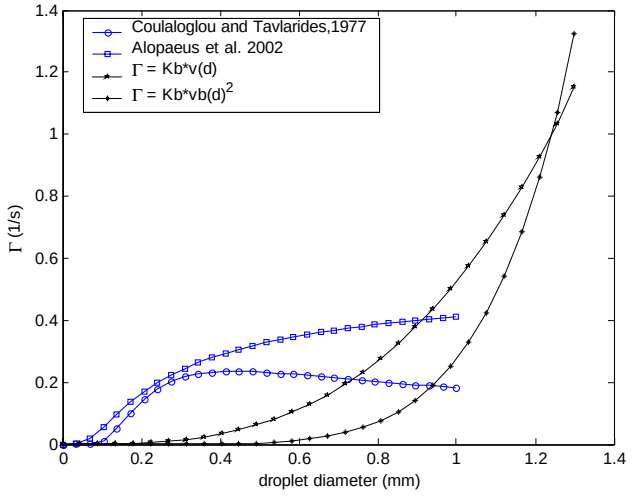

Fig. 4. The behavior of different breakage frequency functions using the physical properties and the energy input specification for cases 3 and 4 and $k_b = 1$ for cases 1 and 2.

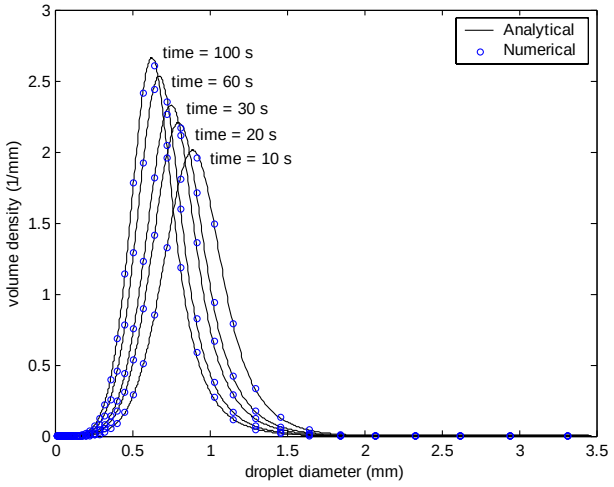

Fig. 5. The dynamic evolution of the droplet volume density: $\Gamma(d) = k_b(\pi d^3/6)$ with $k_b = 1$, $\tau = 100$ s, and $M_x = 50$.

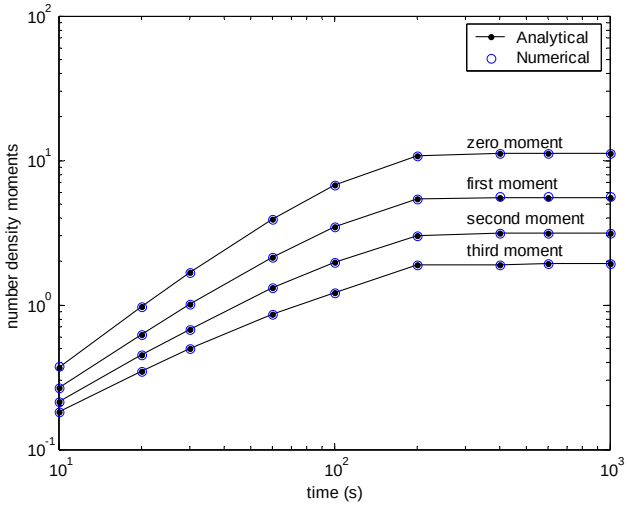

Fig. 6. The dynamic evolution of the number density moments: $\Gamma(d) = k_b(\pi d^3/6)$ with $k_b = 1$, $\tau = 100$ s, and $M_x = 50$.

under the same conditions used in case 1. The sharp changes in the upper size range are also evident in this figure due to the presence of considerable differences in the breakage frequencies when passing from large to small size ranges. This is also clear by referring to Fig. 7a where both cases 1 and 2 are compared at steady sate. The close agreement between the analytical and the predicted solutions are also evident.

Figs. 3–6 show the zero, first, second, and third moments of the predicted and the analytical solutions as calculated by Eq. (54) over the period, $t \in [10, 10\tau]$ for cases 1 and 2. Two important features are revealed by Fig.6 when compared to Fig. 3: the first one is that the steady state is approached faster in case 2 than in case 1 as predicted by the breakage time constants given by Eq. (51) for $p = 1$ and 2, respectively. The second feature is the difference in the magnitude of the zero moments representing the total droplet concentration for the two cases. Again, since the breakage rate for the droplets having diameter $d < 1.5$ mm (refer to Fig. 4) is much smaller in case 2 than that in case 1, and since the droplet distribution is shifted to the left, it is expected that the total number of droplets produced in the second case is much smaller than that in the first one.

9.2. Realization of the present discretization approach

In the previous section we have validated theoretically the performance of the present discretization approach. Before the approach is said to be acceptable we would like to realize it through an application to real cases describing the

droplet evolution in interacting liquid–liquid dispersions. For this purpose the breakage frequencies of Coulaloglou and Tavlarides (1977) and Alopaeus et al. (2002) are used in cases 3 and 4 below.

The inlet feed droplet distribution is chosen as log normal distribution according to Valentas et al. (1966) with mean droplet diameter 0.3 mm and standard deviation of 0.1.

In this realization phase a perfectly mixed industrial scale vessel is considered where the vessel specifications and the two phases physical properties are taken from the work of Alopaeus et al. (1999).

9.2.1. Case 3: Coulaloglou and Tavlarides (1977) breakage frequency

In this case study the breakage frequency of Coulaloglou and Tavlarides (1977) is used (see Table 1). The model is based on the fact that the agitation power dissipated into the continuous phase imparts a distribution of energies and sizes to the turbulent eddies. These eddies interact with the dispersed phase droplets and hence determine the rate at which a given size of droplet will break. This breakage frequency is plotted in Fig. 4 showing a maximum value at about 0.5 mm droplet diameter (Tsouris and Tavlarides, 1994). The actual droplet diameter of the experimentally operated perfectly mixed vessels ranges from 0.1 to 0.6 mm for some cases (Coulaloglou and Tavlarides, 1977) and from 0.1 to 0.4 mm for other cases (Alopaeus et al., 2002). However, in this case study and the other one that will follow a larger droplet diameter is used because of the inlet feed distribution. So, the maximum and minimum droplet diameters are initially estimated using Eqs. (3) and (5) and then refined such that the total droplet number and volume lying outside this range is less than 0.1% over the whole simulation period $t \in [0, 20\tau]$. Values of $d_{\min} = 0.025$ mm and $d_{\max} = 0.9$ mm are found to satisfy the aforementioned criterion at impeller speed of 0.5 s^{-1}. The daughter droplet distribution is chosen as the beta distribution with $\vartheta = 2$ for binary breakage and is given in Table 1.

Since analytical solution is not available for this case study, a numerical solution based on Eq. (53) using a very fine grid of 250 subdomains is considered as the base for the numerical comparisons. Fig. 7b shows the steady state volume droplet distribution using 50 subdomains where this solution seems to be indistinguishable from the base solution using fine grid of 250 subdomains. Due to the relative decrease in the breakage frequency after approximately $d = 0.5$ mm (refer to Fig. 4), the droplet distribution given in Fig. 7b is not very sharp.

9.2.2. Case 4: Alopaeus et al. (2002) breakage frequency

In this case, we used the recently developed droplet breakage frequency (Alopaeus et al., 2002) that takes into account simultaneously both the droplet surface and viscous energies as shown in Table 1. We used the same inlet feed and daughter droplet distributions as in case 3. The numerical

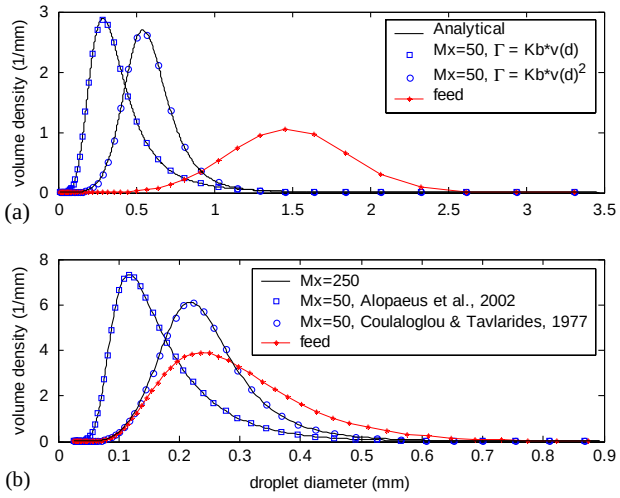

Fig. 7. The steady state droplet volume distribution using the present discretization approach with $\tau = 100$ s : (a) cases 1 and 2 with $k_b = 1$, (b) cases 3 and 4.

parameters, the initial condition, and the energy input are also the same as in case 3. Fig. 7b shows the steady state volume distribution using two levels of discretization: the first one is of 250 subdomains and is considered as the base solution since no analytical one is available. The second level of discretization is of 50 subdomains and it is clear that the two solutions are almost indistinguishable. In this case the volume density is sharper than that of case 3 in the small and in the large size ranges. This is because the present breakage frequency as is evident from Fig. 4 is higher in magnitude than that given by Coulaloglou and Tavlarides (1977) and it is monotone increasing for all $d \in [d_{\min}, d_{\max}]$. Also we studied in this case the effect of the shape of the daughter droplet distribution on the steady state volume density. Fig.8a compares the two steady state volume densities with normal and beta daughter droplet distributions for binary breakage ($\vartheta = 2$). The normal daughter droplet distribution tends to produce sharper distribution than the beta daughter droplet distribution. This behavior is attributed to the sharp form of the normal distribution when compared to the beta distribution; however, the difference is not so large.

10. The convergence of the present discretization approach and the GFP

In the previous four case studies we have presented only qualitative comparisons between the analytical (when it is available) and the predicted solutions, and the predicted solution on relatively coarse and fine grids (when the analytical solution is not available). In this section we would like to investigate thoroughly the quantitative convergence characteristics of the present discretization approach and the generalized fixed-pivot technique since they belong to the same discretization framework. It seems that the systematic error representing the difference between the analytical and the

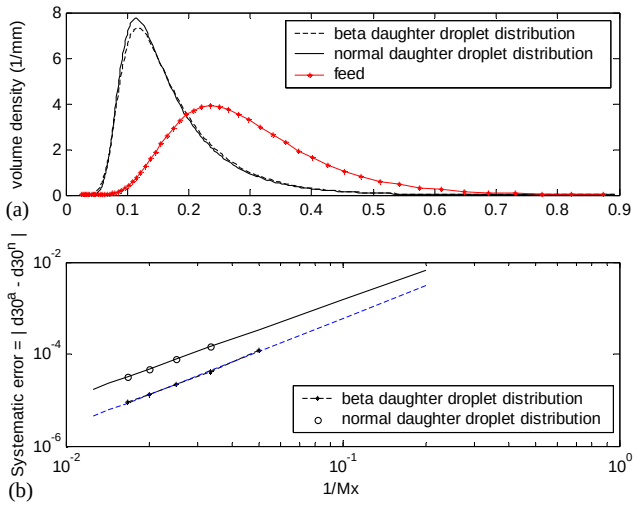

Fig. 8. The effect of daughter droplet distribution on: (a) the steady state droplet volume for case 4 with $\tau = 100$ s. (b) the systematic error for case 4 with $\tau = 100$ s.

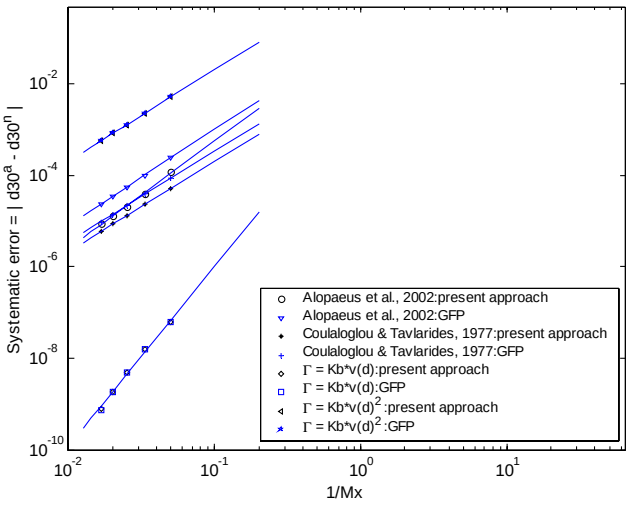

Fig. 9. The convergence characteristics of the present discretization approach and the GFP technique as measured by the systematic error for cases 1, 2, 3, and 4 at steady state with $\tau = 100$ s.

predicted d30 at steady state is a suitable measure to study the convergence characteristics (Attarakih et al., 2003a):

$$\text{SysErr} = |d30^a - d30^n| = K\left(\frac{1}{M_x}\right)^{\alpha}, \tag{55}$$

where K is some constant and α is called the order of convergence and it is expected to depend on the discretization method as well as on the sharpness of the distribution. If the second equality is valid, then a straight line is expected if the above relation is plotted on log–log paper with a slope α estimating the order of convergence. It should be emphasized that in cases where analytical solution is not available we will use the representative droplet diameter, d30, based on the fine grid of 250 subdomains for cases 3 and 4 above.

We will start our discussion from the last case above (case 4) and we will show the effect of the daughter droplet distribution on the systematic error given by Eq. (55). Fig. 8b shows the systematic error versus the inverse of the number of subdomains (intervals) on a log–log scale. First it is clear that the plot is linear with an approximate slope of 2, although the magnitude of the slope in the case of beta distribution is a little bit higher. Also the magnitude of the systematic error in this case is lower than that of the normal distribution due to the difference in the sharpness of the two volume density curves (Fig. 8a).

Fig. 9 shows the convergence characteristics of the present discretization approach and the GFP for the four cases studied above. First, it is clear that all the systematic errors of the four cases produced straight lines when plotted on a log–log scale elucidating the validity of the proposed relation given by Eq. (55). Second, all these straight lines having slopes of magnitudes ranging between 2 and 2.36 except case 1 that has a slope of magnitude 4. As stated previously, the magnitude of the exponent α in Eq. (55) depends on the sharpness of the distribution where it is expected to be large for smooth and symmetric distributions as it is the case in Fig. 7a for case 1. Consequently, it could be concluded that the convergence rate of the present discretization approach is approximately proportional to $(1/M_x)^2$. This result agrees well with the convergence rate of the moving pivot technique (Attarakih et al., 2003a). Third, the convergence of the present approach and the generalized fixed-pivot (GFP) are almost the same for cases 1 and 2, while the present approach has a smaller systematic error than the GFP for cases 3 and 4. This improved convergence of the present approach might be attributed to the different behavior of the breakage frequency functions as shown in Fig. 4, where the breakage frequencies of cases 3 and 4 change sharply in the small size range (when compared to cases 1 and 2) resulting in a sharp droplet distribution in this range. So, it might be concluded that the present discretization approach is superior to the GFP when sharp changes are encountered particularly in the small size range. It is also worthwhile to mention here that the magnitude of the systematic error is less than 10^{-3} for the most cases investigated in this work even when only 15 subdomains are used (refer to Fig. 9). This makes the present approach or the GFP a powerful tool for detailed modeling of the liquid–liquid dispersions by coupling the PBE with computational fluid dynamics (CFD) where complex transport equations are needed.

11. The CPU time

In this section we compare the execution times for the present discretization approach and the GFP technique using two different aspects: first, the CPU time of generating the breakage matrices for the two approaches, and second the execution time of the integration algorithm. The importance of the breakage matrix is to decouple the time-dependent

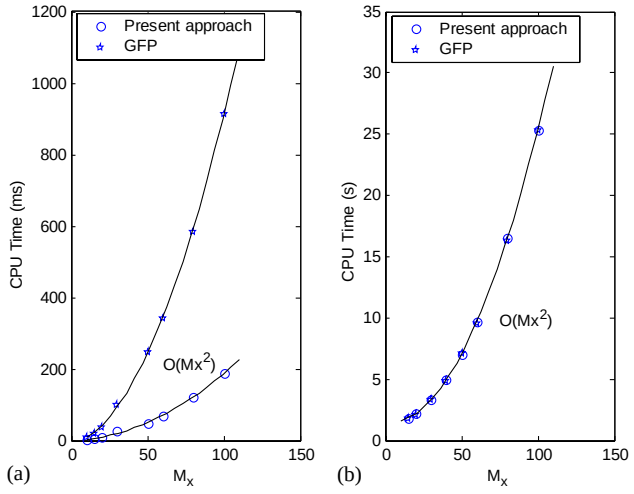

Fig. 10. The CPU time requirements for the present discretization approach and the GFP technique using the problem specification of case 4 for: (a) the generation of the breakage matrix. (b) the integration algorithm using $\Delta t = 1$ s and final simulation time = 800 s.

variables $(N_i(t), \Gamma(d_i, \phi(t)))$ from the simple integrals appearing in Eqs. (25) and (40) for the GFP technique and the present discretization approach, respectively. This allows the breakage matrix to be generated off line and hence the computational time will be considerably reduced. All the runs for the estimation of the CPU time requirements are performed on a PC with Pentium III processor of 700 MHz speed performing a single task. Case 3 is chosen as a real breakage problem to estimate the CPU times as is shown in Fig.10 where the simulation is carried out over a period of time $t \in [0, 8\tau]$ using an integration time step of 1 s and $\tau = 100$ s . Fig. 10a shows the CPU time required to generate the breakage matrices for the present and the GFP technique as a function of number of subdomains (pivots). All the integrals appearing in Eqs. (25) and (40) are performed numerically using a 5-point Gauss quadrature. It is clear that the breakage matrix of the present approach requires shorter computational times than that required by the GFP technique. This is because we only have a single integral in the present discretization approach plus simple algebraic expression given by Eq. (40), while we have two single integrals in the GFP technique. Fig. 10b shows identical CPU requirements for the present approach and the GFP technique. This is not surprising, since once the breakage matrices are generated, the two approaches become exactly identical from the computational point of view. It is also worthwhile to mention here that the CPU time requirement for the generation of the breakage matrices or for integration is proportional to the square of the number of subdomains (pivots).

12. Conclusions

1. A general mathematical approach using the subdomain method is utilized to discretize the general PBE for droplet breakage describing the hydrodynamics of interacting liquid–liquid dispersions in a continuously stirred vessel. The discretization approach presents itself to be computationally efficient since the resulting set of ODEs is free from the evaluation of any double integrals. Moreover, the careful treatment of the breakage matrix makes it possible to decouple the time-dependent variables from the repeated evaluation of the single integrals appearing in the discrete equations.
2. The resulting set of discrete equations (using the subdomain method) is shown to be only internally consistent with respect to one integral property associated with the number density. Based on any two conserved integral properties internal consistency is enforced by introducing a set of auxiliary functions that are uniquely determined.
3. The concept of intrinsic discretization error (IDE) is introduced to show that an exact conservation of two integral properties in all the discrete subdomains (intervals) is not possible. It is also shown quantitatively that the present approach enjoys a lower value of IDE than that of the generalized fixed-pivot.
4. The present discretization approach is validated through comparing its predictions with two analytical solutions of the problem at hand. The numerical results seem to agree well with the analytical solutions for both the volume density and some selected moments. Realization of the approach is performed using two experimentally validated breakage frequency functions, as well as two daughter droplet distributions. For these cases the predicted dispersed phase hold up is found to agree to a very good extent with the exact solutions.
5. The convergence characteristics of the present approach are found identical to that of the generalized fixed-pivot technique and in some cases they are even better than it. The order of convergence is found to be approximately proportional to $(1/M_x)^2$ in spite of its dependence on the sharpness of the distribution. The results show that 15–20 subdomains (intervals) are sufficient to produce acceptable predictions when the hydrodynamics of liquid–liquid dispersions is considered.
6. The discrete set of equations of the present approach is independent of the grid structure and hence allowing selective grid refinement as well as the coupling of this approach with the fixed-pivot technique for droplet coalescence.

Notation

B	London–van der Waals constant, Jm
B_o	linear droplet breakage operator as defined in Eq. (12)
d, d'	droplet diameter, m
$d_{\min}, d_{\max}$	minimum and maximum droplet diameters, m
d_i	the characteristic droplet diameter in the ith subdomain, m

d_0 parameter in for the inlet feed distribution, m
$d30$ representative droplet diameter defined as $\left(\int_{d_{\min}}^{d_{\max}} d^3 n(d,t)\delta d / \int_{d_{\min}}^{d_{\max}} n(d,t)\delta d\right)^{1/3}$, m
$d30^a, d30^n$ analytical and numerical $d30$, respectively
D_R impeller diameter, m
erfc complementary error function
$F(t), F_i(t)$ integral properties defined as $\int_{v_{\min}}^{v_{\max}} u_m(v)n(v,t)\,\mathrm{d}v$, $\int_{v_{i-1/2}}^{v_{i+1/2}} u_m(v)n(v,t)\,\mathrm{d}v$
IDE intrinsic discretization error as defined in Eq. (27)
K empirical constant appearing in Eq. (55)
L differential operator as defined in Eq. (13)
M_x total number of subdomains (intervals) used in droplet volume discretization
$M_j(t)$ the jth moment associated with the number density, $n(d,t)$
$n(v,t)\,\mathrm{d}v$ number of droplets in size range v to $v+\mathrm{d}v$ at time t
$n^{\mathrm{feed}}(v,t)\,\mathrm{d}v$ number of droplets in the inlet feed in size range v to $v+\mathrm{d}v$ at time t
$N(t)$ total number of droplets per unit volume of the dispersion at time t, m^{-3}
$N_i(t)$ total number of droplets in the ith subdomain (interval) per unit volume at time t, m^{-3}
N^{feed} total number of droplets in the inlet feed per unit volume, m^{-3}
N_0^f parameter for the inlet feed distribution, m^{-3}
$p(d,t)\delta d$ volume of droplets in the size range d to $d+\delta d$ at time t
SysErr systematic error as defined in Eq. (55)
t time, s
u_m the mth desired integral property associated with the number droplet distribution
v, v' droplet volumes, m^3
$v_{\min.}, v_{max.}$ minimum and maximum droplet volumes, m^3
V vessel volume, m^3
w_k unit step function in the kth subdomain as defined in Eq. (11)
We Weber number ($\rho_{\mathrm{disp.}} N^2 D_R^3/\sigma$)
x_i characteristic droplet volume in the ith subdomain

Greek letters

α order of convergence as appears in Eq. (55)
$\beta_n(v|v')\mathrm{d}v$ fractional number of droplets formed in the size range v to $v+\mathrm{d}v$ formed upon breakage of droplet of volume v'
$\Gamma(v)$ number of droplets in the size range v to $v+\mathrm{d}v$ disappearing per unit time by breakage
$\gamma_i^{<i>}$ fraction of droplets from the interval $[x_i, x_{i+1})$ that is assigned to the pivot x_i
$\gamma_i^{<i-1>}$ fraction of droplets from the interval $[x_{i-1}, x_i)$ that is assigned to the pivot x_i
δ Dirac delta function
ε average turbulent energy dissipated in the continuous phase, $\mathrm{m}^2\ \mathrm{s}^{-3}$
$\eta(x_i)$ auxiliary function as defined in Eq. (39)
$\pi_{i,k}^{<m>}$ breakage matrix as defined in Eq. (25)
μ_c, μ_d viscosity of the continuous and dispersed phases respectively, $\mathrm{kg\ m}^{-1}\ \mathrm{s}^{-1}$
ρ the source term describing droplet breakage and coalescence as appears in Eq. (1)
ρ_c, ρ_d density of the continuous and dispersed phases, respectively, $\mathrm{kg\ m}^{-3}$
σ interfacial tension, $\mathrm{N\ m}^{-1}$
$\sigma(x_i)$ auxiliary function as defined in Eq. (38)
τ vessel time constant, s
$\vartheta(v')$ average number of droplets produced when mother droplet of volume, v', is broken
$\phi, \phi^{\mathrm{feed}}$ the dispersed phase hold up in the vessel and the feed, respectively

Acknowledgements

The authors wish to thank the DFG (Deutsche Forschungsgemeinschaft) and DAAD (Deutscher Akademischer Austauschdienst) for supporting this work.

Appendix A. Analytical solution of the unsteady state breakage equation in a continuous flow vessel (special case)

We start solving analytically the unsteady state breakage equation by introducing the dimensionless variable $z = v/v_0$ and the new density function $f(z,t) = v_0 n(v,t)/N_0^f$ into Eq. (2):

$$\frac{\partial f(z,t)}{\partial t} = \frac{1}{\tau}(f^{\mathrm{feed}}(z,t) - f(z,t)) - \Gamma(z)f(z,t) + \int_z^\infty \Gamma(z')\beta_n(z|z')f(z',t)\,\mathrm{d}z' \quad (A.1)$$

where

$$\Gamma(z) = z^p, \quad (A.2)$$

$$f^{\mathrm{feed}}(z) = \mathrm{e}^{-z}, \quad (A.3)$$

$$f(z,0) = 0. \quad (A.4)$$

Taking the Laplace transform of both sides of Eq. (A.1) with respect to t and let $F(z,s)$ be the Laplace transform of $f(z,t)$ one could obtain

$$(a(z) + \tau s)F(z,s) = F^{\mathrm{feed}}(z,s) + 2\tau \int_z^\infty (z')^{p-1} F(z',s)\,\mathrm{d}z', \quad (A.5)$$

where

$$a(z) = 1 + \tau z^p. \tag{A.6}$$

Following Nicmanis and Hounslow (1998), Eq. (A.5) is an integral equation and could be transformed to a first order linear ODE by differentiating it with respect to z and after some algebraic manipulation we get

$$\frac{\mathrm{d}F(z,s)}{\mathrm{d}z} + \frac{(p+2)\tau z^{p-1}}{a(z)+\tau s} F(z,s) = \left(\frac{1}{a(z)+\tau s}\right) \frac{\mathrm{d}F^{\mathrm{feed}}(z,s)}{\mathrm{d}z}. \tag{A.7}$$

The initial condition for this ODE could be obtained by setting $z = 0$ in Eq. (A.5) to get

$$F_p(0,s) = \left(\frac{2\tau}{1+\tau s}\right) M_{p-1}(s) + \frac{F^{\mathrm{feed}}(0,s)}{1+\tau s}, \tag{A.8}$$

where $M_{p-1}(s)$ is the Laplace transform of the $(p-1)$th moment of the function $F(z,s)$ which could only be obtained for the two special cases when $p = 1$ and 2. This is because the higher order moments ($p > 2$) of the breakage equation (Eq. (A.1)) are unclosed according to the following equation:

$$M_m(s) = \frac{\tau}{1+\tau s}\left(\frac{2}{m+1} - 1\right) M_{m+p}(s) + \frac{\tau}{1+\tau s} M_m^{\mathrm{feed}}(s), \quad m = 0, 1, \ldots. \tag{A.9}$$

So, for p=1, and 2 we have to find expressions for $M_0(s)$ and $M_1(s)$ as required by Eq. (A.8). These expressions follow directly from the last equation by setting $m = 0$ when $p = 1$ and $m = 1$ when $p = 2$:

$$M_1(s) = \frac{1}{1+\tau s} M_1^{\mathrm{feed}}(s), \tag{A.10}$$

$$M_0(s) = \frac{1}{1+\tau s} M_0^{\mathrm{feed}}(s) + \frac{\tau}{1+\tau s} M_1(s). \tag{A.11}$$

So the initial condition given by Eq. (A.8) is now completely defined for $p = 1$ and $p = 2$.

The integration factor for Eq. (A.7) could be easily obtained as follows:

$$I(z,s) = \exp\left((p+2)\tau \int_0^z \frac{z'^{p-1}}{a(z)+\tau s}\,\mathrm{d}z'\right) = (a(z)+\tau s)^{p+2/p}. \tag{A.12}$$

Now the complete solution of Eq. (A.7) using the feed distribution as given by Eq. (A.3) could be written with the aid of this integration factor as

$$F(z,s) = \frac{(1+\tau s)F_p(0,s)}{(a(z)+\tau s)^{(p+2)/p}} - \frac{1}{(a(z)+\tau s)^{(p+2)/p}} \int_0^z \frac{(a(z')+\tau s)^{(2/p)}\mathrm{e}^{-z'}}{s}\,\mathrm{d}z'. \tag{A.13}$$

The integral on the left-hand side of this equation could be evaluated depending on the values of $p = 1$ and 2 so one could obtain the following two solutions:

$$F(z,s) = \frac{\mathrm{e}^{-z}}{s(a(z)+\tau s)} + \frac{2\tau \mathrm{e}^{-z}}{s} \times \left(\frac{\tau}{(a(z)+\tau s)^3} + \frac{1}{(a(z)+\tau s)^2}\right), \quad \text{for } p = 1, \tag{A.14}$$

$$F(z,s) = \frac{\tau \mathrm{e}^{-z}}{(a(z)+\tau s)^2} + \left(\frac{1+\tau+\tau(1+z)^2}{s(a(z)+\tau s)^2}\right)\mathrm{e}^{-z}, \quad \text{for } p = 2. \tag{A.15}$$

The inversion of Eqs. (A.14) and (A.15) from the Laplace domain to the time domain is straightforward but it involves a tedious and lengthy algebra. Therefore, we used Mathcad7 software to symbolically perform these operations. We finally got the complete analytical solutions of Eq. (A.1) using the following relation for transforming the resulting equations from the droplet volume into diameter coordinates:

$$n(d,t) = \frac{3d^2 N_0^f}{d_0^3} f(z,t). \tag{A.16}$$

The complete analytical solution is given by Eqs. (46)–(52) for the two special cases described above.

References

Alopaeus, V., Koskinen, J., Keskinen, K.I., 1999. Simulation of population balances for liquid–liquid systems in a nonideal stirred tank. Part 1: description and qualitative validation of model. Chemical Engineering Science 54, 5887–5899.

Alopaeus, V., Koskinen, J., Keskinen, K.I., Majander, J., 2002. Simulation of population balances for liquid–liquid systems in a nonideal stirred tank. Part 2 parameter fitting and the use of the multiblock model for dense dispersion. Chemical Engineering Science 57, 1815–1825.

Attarakih, M.M., Bart, H.J., Faqir, M.M., 2002. An approximate optimal moving grid technique for the solution of discretized population balances in batch systems. In: Grievink, J., Schijndel van, J. (Eds.), European Symposium on Computer Aided Process Engineering-12, Computer-Aided Chemical Engineering, Vol. 10. Elsevier, Amsterdam, pp. 823–828.

Attarakih, M.M., Bart, H.-J., Faqir, N.M., 2003a. Optimal moving and fixed grids for the solution of discretized population balances in batch and continuous systems: droplet breakage. Chemical Engineering Science 58, 1251–1269.

Attarakih, M.M., Bart, H.-J., Faqir, N.M., 2003b. Solution of the population balance equation for liquid–liquid extraction columns using a generalized fixed-pivot and central difference schemes. In: Kraslawski, A., Turunen, I. (Eds.), European Symposium on Computer Aided Process Engineering-13, Computer-aided chemical engineering, Vol. 14. Elsevier, Amsterdam, pp. 557–562.

Attarakih, M.M., Bart, H.-J., Faqir, N.M., 2004. Numerical solution of the spatially distributed population balance equation describing the hydrodynamics of interacting liquid–liquid dispersions. Chemical Engineering Science, this issue.

Gelbard, F., Seinfeld, J.H., 1978. Numerical solution of the dynamic equation for particulate systems. Journal of Computer Physics 28, 357–375.

Gelbard, F., Tambour, Y., Seinfeld, J.H., 1980. Sectional representation of simulating aerosol dynamics. Journal of Colloid and Interface Science 76, 541–556.

Hill, P.J., Ng, K.M., 1995. New discretization procedure for the breakage equation. A.I.Ch.E. J. 41, 1204–1216.

Hounslow, M.J., Ryall, R.L., Marshall, V.R., 1988. A discretized population balance for nucleation, growth, and aggregation. A.I.Ch.E. J. 34, 1821–1832.

Kostoglou, M., Karabelas, A.J., 1994. Evaluation of zero order methods for simulating particle coagulation. Journal of Colloid and Interface Science 163, 420–431.

Kostoglou, M., Karabelas, A.J., 1995. Evaluation of numerical methods for simulating an evolving particle size distribution in growth processes. Chemical Engineering Communication 136, 177–199.

Kronberger, T., 1995. Numerische Simulation von Tropfenpopulationen in Extraktionskolonnen, Dissertation, Johannes Kepler Universitat Linz, Linz.

Kronberger, T., Ortner, A., Zulehner, W., Bart, H., 1995. Numerical simulation of extraction columns using a drop population model. Computers and Chemical Engineering 19, S639–S644.

Kumar, S., Ramkrishna, D., 1996a. On the solution of population balance equations by discretization-I. A fixed pivot technique. Chemical Engineering Science 51, 1311–1332.

Kumar, S., Ramkrishna, D., 1996b. On the solution of population balance equations by discretization-II. A moving pivot technique. Chemical Engineering Science 51, 1333–1342.

Lister, J.D., Smit, D.J., Hounslow, M.J., 1995. Adjustable discretized population balance for growth and aggregation. A.I.Ch.E. J. 41, 591–603.

Liu, S., Li, D., 1999. Drop coalescence in turbulent dispersions. Chemical Engineering Science 54, 5667–5675.

Mahoney, A.W., Ramkrishna, D., 2002. Efficient solution of population balances equations with discontinuities by finite elements. Chemical Engineering Science 57, 1107–1119.

McGrady, E.D., Ziff, R.M., 1988. Analytical solutions to fragmentation equation with flow. A.I.Ch.E. J. 34, 2073–2076.

Nambiar, D.K.R., Kumar, R., Das, T.R., Gandhi, K.S., 1992. A new model for the breakage frequency of drops in turbulent stirred dispersions. Chemical Engineering Science 47, 2989–3002.

Nicmanis, M., Hounslow, M.J., 1998. Finite-element methods for steady-state population balance equations. A.I.Ch.E. J. 44, 2258–2272.

Ramkrishna, D., 1985. The status of population balances. Reviews in Chemical Engineering 3, 49–95.

Ramkrishna, D., 2000. Population Balances. Academic Press, San Diego.

Ribeiro, L.M., Regueiras, P.F.R., Guimaraes, M.M.L., Madureira, C.M.C., Cruz-Pintu, J.J.C., 1995. The dynamic behavior of liquid–liquid agitated dispersions-I. The hydrodynamics. Computers and Chemical Engineering 19, 333–344.

Rice, G.R., Do, D.D., 1995. Applied Mathematics and Modeling for Chemical Engineers. Wiley, New York.

Shah, B.H., Ramkrishna, D., 1973. A population balance model for mass transfer in lean liquid–liquid dispersions. Chemical Engineering Science 28, 389–399.

Tsouris, C., Tavlarides, L.L., 1994. Breakage and coalescence models for drops in turbulent dispersions. A.I.Ch.E. J. 40, 395–406.

Valentas, K.J., Bilois, O., Amundson, A.R., 1966. Analysis of breakage in dispersed phase systems. Industrial Engineering and Chemical Fundamentals 5, 271–279.

Vanni, M., 1999. Discretization procedure for the breakage equation. A.I.Ch.E. J. 45, 916–919.

Vanni, M., 2000. Approximate population balances equations for aggregation-breakage processes. Journal of Colloid and Interface Science 221, 143–160.